Single-particle analysis reveals shutoff control of the *Arabidopsis* ammonium transporter AMT1;3 by clustering and internalization

Qinli Wang[a,1], Yuanyuan Zhao[a,1], Wangxi Luo[b], Ruili Li[a], Qihua He[c], Xiaohong Fang[b], Roberto De Michele[d,e], Cindy Ast[d], Nicolaus von Wirén[f], and Jinxing Lin[a,2]

[a]Key Laboratory of Plant Molecular Physiology, Institute of Botany, Chinese Academy of Sciences, Beijing 100093, China; [b]Institute of Chemistry, Chinese Academy of Sciences, Beijing 100190, China; [c]Peking University Health Science Center, Beijing 100191, China; [d]Department of Plant Biology, Carnegie Institution for Science, Stanford, CA 94305; [e]Institute of Plant Genetics, National Research Council of Italy, 90123 Palermo, Italy; and [f]Leibniz Institute for Plant Genetics and Crop Plant Research, 06466 Gatersleben, Germany

Ammonium is a preferred source of nitrogen for plants but is toxic at high levels. Plant ammonium transporters (AMTs) play an essential role in NH_4^+ uptake, but the mechanism by which AMTs are regulated remains unclear. To study how AMTs are regulated in the presence of ammonium, we used variable-angle total internal reflection fluorescence microscopy and fluorescence cross-correlation spectroscopy for single-particle fluorescence imaging of EGFP-tagged AMT1;3 on the plasma membrane of *Arabidopsis* root cells at various ammonium levels. We demonstrated that AMT1;3-EGFP dynamically appeared and disappeared on the plasma membrane as moving fluorescent spots in low oligomeric states under N-deprived and N-sufficient conditions. Under external high-ammonium stress, however, AMT1;3-EGFPs were found to amass into clusters, which were then internalized into the cytoplasm. A similar phenomenon also occurred in the glutamine synthetase mutant *gln1;2* background. Single-particle analysis of AMT1;3-EGFPs in the clathrin heavy chain 2 mutant (*chc2* mutant) and *Flotllin1* artificial microRNA (*Flot1 amiRNA*) backgrounds, together with chemical inhibitor treatments, demonstrated that the endocytosis of AMT1;3 clusters induced by high-ammonium stress could occur mainly through clathrin-mediated endocytic pathways, but the contribution of microdomain-associated endocytic pathway cannot be excluded in the internalization. Our results revealed that the clustering and endocytosis of AMT1;3 provides an effective mechanism by which plant cells can avoid accumulation of toxic levels of ammonium by eliminating active AMT1;3 from the plasma membrane.

VA-TIRFM | FCS

Ammonium (NH_4^+) and nitrate (NO_3^-) are the primary sources of nitrogen (N) for most plants growing in agricultural soils. Ammonium assimilation requires less energy than nitrate assimilation, and, thus, ammonium is absorbed preferentially when plants are N-deficient. However, high concentrations of ammonium can be toxic (1); therefore, ammonia absorption and metabolism must be strictly controlled. Understanding the mechanisms by which plant cells regulate ammonium uptake and translocation is of critical importance for agricultural improvements in N-use efficiency and avoiding ammonium toxicity.

Evidence suggests that membrane ammonium transporters (AMTs) act in NH_4^+ uptake into plant cells, serving as the major transporters for high-affinity ammonium uptake (2). In *Arabidopsis thaliana*, the AMT family comprises six isoforms, of which three (AtAMT1;1, AtAMT1;2, and AtAMT1;3) are responsible for about 90% of the total high-affinity N uptake in roots (3). AMT gene expression in *Arabidopsis* roots is generally repressed by high N and induced by N deficiency (4). In addition to transcriptional mechanisms, regulation of membrane transporter activity is also involved in the plant's responses to changing nutrient supplies (1). Although posttranscriptional regulation of AMT

appears to be N-dependent (5), the question of how ammonium regulates AMT transporter activity, particularly the initial events that take place immediately after the addition of ammonium, remains to be characterized.

It is difficult to unambiguously determine the behavior and character of individual molecules in living cells by means of bulk methods because these can only provide "average data" across many millions of molecules. However, single-molecule techniques have been recently used to reveal new information that would otherwise be lost in averages (6, 7). For example, variable-angle total internal reflection fluorescence microscopy (VA-TIRFM) can detect individual molecules of membrane-associated proteins with fast dynamics in intact plant cells (8). Fluorescence-correlation spectroscopy (FCS) allows direct measurements in living cells to estimate densities of live cell membrane proteins in their native environment without affecting protein function (9). Dual-color fluorescence cross-correlation spectroscopy (FCCS) is an extension of FCS that can quantitatively estimate molecule–molecule interactions in living cells (10). The combination of these single-molecule techniques greatly facilitates identification and characterization of single-membrane protein molecules.

In this investigation, we used these single-particle approaches to investigate the behavior of individual molecules of AMT1;3 in living roots of transgenic *Arabidopsis* expressing an *AMT1;3-EGFP* construct. We found that cells respond to high-ammonium stress by clustering these transporter proteins and subsequently internalizing the transporters, thereby likely reducing their ammonium-transport capacity. Clathrin-dependent and microdomain-associated pathways are involved in this internalization. Our single-particle analyses offer insights into the shutoff regulation of AMT1;3 transporter to protect against toxic ammonium accumulation under excess-ammonium conditions and may also serve as a model of how membrane transporters control substrate transport.

Results and Discussion

In plant roots, transport of ammonium across membranes is mainly mediated by the AMTs, and AMT expression and activity are regulated in response to the changing ammonium supply (5, 11). Evidence suggests that the behavior of individual molecules is of particular importance because it can be correlated to the environmental conditions (12). It has been reported that AMT1;3 is widely distributed in the epidermal cells of *Arabidopsis* roots and makes an important contribution to the absolute ammonium uptake capacity (2, 3). By contrast, AMT1;1 is mostly localized in the pericycle cells, and AMT1;2 is found in endodermis and cortex cells. Because AMT1;3 is expressed in the epidermal cells of *Arabidopsis* roots (2, 3, 13), we, therefore, selected AMT1;3 as a representative protein to track the dynamic behavior of ammonium transporters under different external ammonium conditions. We first confirmed that AMT1;3-EGFP is functional by a complementation assay in yeast (Fig. S1) and also showed that it localized at the plasma membrane in root epidermal cells (Fig. S2 *A–L*).

At low or null ammonium concentrations, the fluorescence of AMT1;3-EGFP spots exhibited heterogeneous dynamic modes with different surface residence times (Fig. 1*A*). One typical dynamic mode is the spots appeared and then immediately disappeared from the cell cortex (Fig. 1*B*, M1 mode). In another common dynamic mode, the spots had a long membrane residence time before they completely disappeared (Fig. 1*B*, M2 mode). Defining a lifetime of <1 s as short-lived and anything above this threshold as long-lived, our statistical analysis indicated that, at low ammonium concentration (including 2 mM NH_4NO_3, regarded as N-sufficient conditions), 44.5% of AMT1;3-EGFP spots were short-lived and 55.5% of the spots were long-lived (Fig. 1*C* and Movie S1). However, in N-deprived conditions, the long-lived spots increased significantly to 78% (Fig. 1*D* and Movie S2), suggesting that the distribution of surface-residence time of AMT1;3 spots depended on ammonium conditions.

Crystal structure studies have shown that AMT transporters exist as trimers (14); however, because the structure of detergent-isolated proteins may not always reflect the physiologically relevant state (15), it is necessary to directly analyze the oligomeric state of AMTs in living cells. Recent advances in single-molecule fluorescence imaging of living cells have provided a new way to analyze protein structures under physiological conditions (7, 16). Here, we report the native oligomeric status of AMT1;3 based on single-particle fluorescence-imaging analysis. We found that, under low or null ammonium concentrations, AMT1;3-EGFP exhibited a broad asymmetric distribution of intensities, with the majority of spots ranging from 500 to 1,000 counts (Fig. 2*A*), which were approximately one- or twofold that of purified of EGFP monomers (peak intensity at 545; Fig. S3*A*), suggesting that these spots included one or two AMT1;3-EGFP molecules. To circumvent the signal fluctuation attributable to the dynamics of AMT1;3-EGFP on living cell surfaces, we then confirmed the subunit number of AMT1;3 by counting bleaching steps of GFP tags fused to the proteins in fixed cells (Fig. 2*B* and Fig. S3*B*), through a single-molecule photobleaching approach (16). As shown in Fig. 2 *C–E*, the number of elemental EGFP photobleaching steps in an individual spot was not uniform, ranging from one to three. Because the maximum number was three, the most conservative explanation is that that AMT1;3 exists on the membrane as a trimer, in agreement with previous reports (14). The one- or two-step photobleaching may result from oligomers that incorporate endogenous unlabeled AMTs or some AMT1;3-EGFP with an immature EGFP tag. However, another possibility that cannot be excluded is that besides existing as a trimer on the plasma membrane, AMT1;3 may also exist as a mixture of various multimeric forms including monomers, dimers, and trimers.
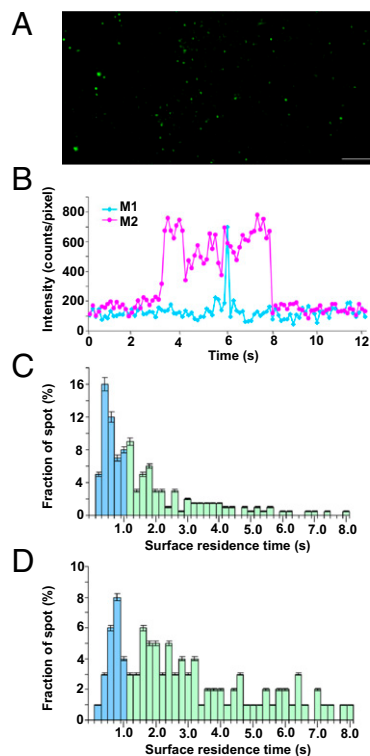
Fig. 1. Dynamic analysis of AMT1;3-EGFP spots in the plasma membrane under N-sufficient conditions, based on VA-TIRFM observation of a total of 200 spots from five representative living *Arabidopsis* roots. To calculate the surface residence time, we measured the changes of fluorescence intensity of AMT1;3 spots over an interval of fixed duration (12 s), with the interval starting first at 0 ms after the beginning of the recording, then 200 ms, 400 ms, and so on until 12 s. (*A*) Typical image showing diffraction-limited fluorescent spots of AMT1;3-EGFP in living expanding *Arabidopsis* root epidermal cells, imaged with VA-TIRFM. (Scale bar: 1 μm.) (*B*) The fluorescence intensity over time of AMT1;3-EGFP spots in two typical dynamic modes. M1, spots that appeared and then immediately disappeared. On first appearance, these spots had low but detectable fluorescence that increased steadily. After reaching a peak fluorescence intensity, the fluorescence rapidly decreased to background levels and the spots disappeared from the cell cortex. M2, spots that disappeared after long-lasting residence in the plasma membrane. (*C*) Surface residence time of 200 AMT1;3-EGFP spots in the plasma membrane in N-sufficient seedlings. A surface residence time of <1 s was defined as short-lived, and anything above this threshold was defined as long-lived (*n* = 200). The data came from three independent replicates. (*D*) Surface residence time of 200 AMT1;3-EGFP spots in the plasma membrane in N-deprived seedlings (*n* = 200). The data came from three independent replicates.

Ammonium provides an essential plant nutrient but is toxic when present in excess. When plants are exposed to high-ammonium conditions, roots undergo a rapid decrease in N-uptake capacity to avoid cellular ammonium toxicity (3). Previous studies reported that the spatial organization of transmembrane proteins is a critical step in signal transduction and protein trafficking, and different multimeric states of the protein complex can result in distinct cellular responses (17). To test whether high-ammonium stress changes AMT1;3 protein organization, we compared the state of individual AMT1;3-EGFP spots under high-ammonium stress (30 mM NH_4^+) and under N-sufficient conditions (2 mM NH_4^+). Our results showed that, under N-sufficient conditions, most of the AMT1;3 transporters existed in low oligomeric states with the average size $2.32 \times 2.32 \pm 0.25$ pixels and fluorescence intensity of 600.5 ± 75 counts per pixel. However, 30 min after transfer to high-ammonium medium, the average size and fluorescence intensity of AMT1;3-EGFP spots
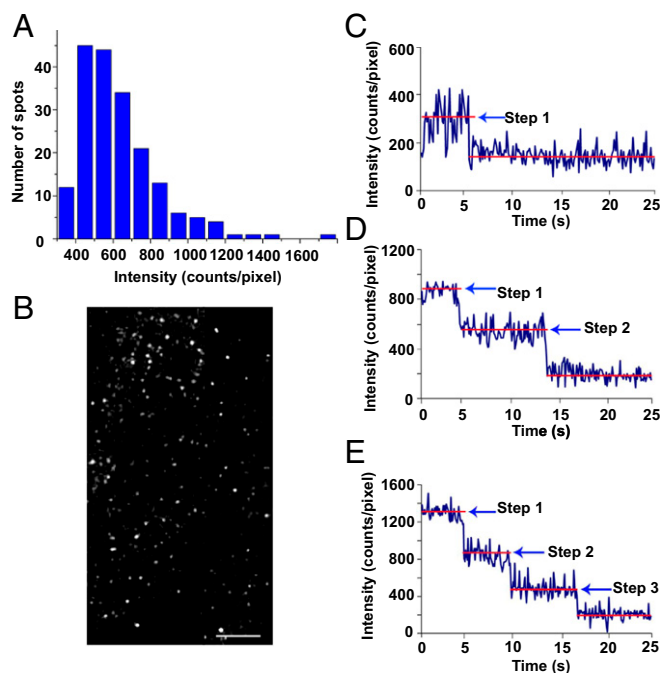
Fig. 2. Analysis of oligomeric states of AMT1;3-EGFP in *Arabidopsis* root cells. (*A*) Distribution of fluorescence intensities of the diffraction-limited single AMT1;3-EGFP spots (*n* = 200) in five live cells from five representative *Arabidopsis* roots. (*B*) Typical image showing diffraction-limited fluorescent spots of AMT1;3-EGFP on fixed cell membrane of *Arabidopsis* root cells, imaged with VA-TIRFM. The image is a section of the first frame of a stack of images with the background subtracted. (Scale bar: 1 μm.) (*C*–*E*) Representative time courses of EGFP emission of AMT1;3-EGFP spots in fixed *Arabidopsis* root cells after background correction: one-step bleaching (*C*), two-step bleaching (*D*), and three-step bleaching (*E*). Movies of 150 frames were captured with a 200-ms frame interval.

significantly increased to 5.38 × 5.38 ± 1.8 pixels and 3,046 ± 502 counts per pixel (*P* < 0.01), respectively, suggesting that AMT1;3 molecules amassed into protein clusters (Fig. 3 *A* and *B*). Additionally, representative time courses of EGFP emission of spots under high ammonium showed that most of the bleaching steps exhibited an exponential decay without discrete steps (Fig. 3*C*), suggesting that each fluorescent spot was a cluster of several AMT1;3-EGFP molecules. Because trimers are believed to be the functional units (14) and abnormal protein complex organization can result in dysfunction (18), these results suggest that the clustering of AMT1;3 induced by high ammonium may play an important role in regulating transporter activity.

It has been reported that clustering can promote subsequent internalization of membrane proteins (19). Thus, we further investigated the fate of the AMT1;3 clusters. Compared with N-sufficient conditions (Fig. 3*D*), whereas the size and fluorescence intensity of spots increased under high-ammonium conditions, the overall number of spots and their residence time dramatically decreased (Fig. 3*E*). During 30 min of high-ammonium supply, only 31.6 ± 1.6% of AMT1;3-EGFP surface fluorescence remained (Fig. 3*H*). This observation, together with the disappearance of individual AMT1;3 spots from the plasma membrane (Movie S3), suggests that at high-ammonium stress, AMT1;3 protein clusters are rapidly internalized. To investigate whether ammonium exerts a specific effect on AMT1;3 localization, we analyzed the cytoplasmic pH of root cells using the Oregon Green 488 fluorescent probe (20) and found that there was no significant difference in cytoplasmic pH in root cells between N-sufficient and high-ammonium conditions (Fig. S4 *A*–*C*; *P* > 0.05), indicating that the effects of ammonium on the localization

and dynamics of AMT1:3 proteins are specific to the ammonium ion rather than a result of its action as a weak base. In addition, treatments with 2 and 30 mM NH$_4$Cl, KNO$_3$, KCl further confirmed that the change of AMT1;3-EGFP behavior did not result from the effects of NO$_3^-$ or osmotic potential (Fig. S5 *A*–*C*). Moreover, we examined the effect of ammonium availability on localization of GFP-PIP2;1 (a plasma membrane aquaporin transporter) and clathrin light chain (CLC)-GFP by confocal microscopy. Although the distribution of GFP-PIP2;1
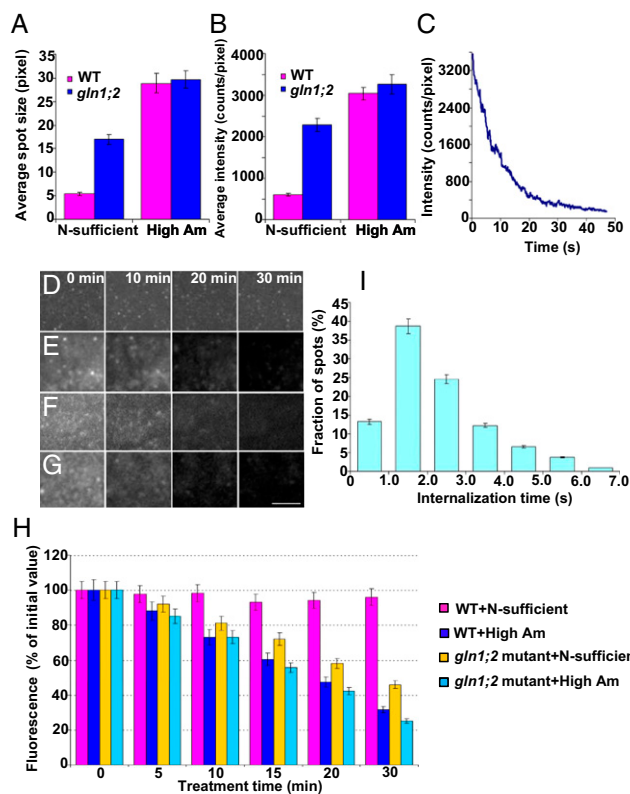

Fig. 3. Dynamic analysis of AMT1;3-EGFP internalization induced by high-ammonium stress in *Arabidopsis* root cells. (*A* and *B*) Average size (*A*) and fluorescence intensity (*B*) of AMT1;3-EGFP fluorescent spots in wild type under N-sufficient conditions and high-ammonium treatment, and in *gln1;2* mutant background under N-sufficient conditions (*n* = 200), showing that external high-ammonium stress and internal ammonium accumulation induced the massing of AMT1;3-EGFP oligomers into clusters. The data came from three separate replicates. Values given are means ± SD. (*C*) Representative time course of EGFP emission of AMT1;3-EGFP spots under high-ammonium stress in fixed *Arabidopsis* root cells after background correction, showing the approximately exponential distribution of the bleaching steps. (*D*–*G*) The raw frames of a representative area of *Arabidopsis* root cells expressing AMT1;3-EGFP, imaged live using VA-TIRFM at the indicated times. (*D*) In wild-type background under N-sufficient condition. (*E*) In wild-type background under high-ammonium stress. (*F*) In *gln1;2* mutant background under N-sufficient conditions. (*G*) In *gln1;2* mutant background under high-ammonium stress. (Scale bar: 1 μm.) (*H*) Corresponding average surface fluorescence measurements in *D*–*G*. In wild type, no distinct change of surface fluorescence was found over a 30-min period under N-sufficient conditions. After high-ammonium treatment, only 31.6 ± 1.6% of AMT1;3-EGFP remained on the membrane surface. In the *gln1;2* mutant, 46 ± 2.7% AMT1;3-EGFP remained under N-sufficient conditions, but only 25.1 ± 1.2% of AMT1;3-EGFP remained on the membrane surface after high-ammonium treatment. Approximately five to eight cells in at least five different seedlings were measured. The analysis was based on three independent repetitions. Values given are means ± SD. (*I*) Analysis of AMT1;3-EGFP endocytic rate (*n* = 200). The fast-spot internalization required only about 0.66 s, whereas slow-spot internalization required about 6.8 s. The analysis was based on three separate replicates. Values given are means ± SD.

(Fig. S6 *A–F*) and CLC-GFP (Fig. S7 *A–F*) remained unaltered under N-sufficient and high-ammonium conditions, more AMT1;3 dot-like endocytic structures occurred in the cytoplasm under high-ammonium stress (Fig. S8 *A–F*), suggesting high-ammonium treatment specifically induced the internalization of AMT1;3 but did not affect the localization of other proteins in general. In addition, we performed Western blot experiments to check the abundance of the AMT1;3-EGFP protein after high-ammonium treatment. Consistent with our expectation, the AMT1;3-EGFP protein underwent sequential degradation (Fig. S9). Using the scanning ion-selective electrode technique (SIET) (21), we demonstrated that the net NH_4^+ uptake rate of roots after treatments with different ammonium concentrations ranked in the following order, from highest to lowest uptake: N-limiting > N-sufficient > high-ammonium treatment (Fig. S10 *A–C*). Therefore, we concluded that the ammonium-induced clustering of AMT1;3, followed by internalization, might work as a shutoff regulatory mechanism that removes active AMT1;3 from the cell surface to protect against accumulation of toxic levels of ammonium.

We were also curious as to whether perturbation of internal ammonium levels could induce a change of AMT1;3 spot behavior. Therefore, a parallel experiment was conducted using the *gln1;2* mutant to produce a treatment-independent effect on the ammonium pathway with different internal ammonium levels, to confirm whether internal ammonium level was related to the dynamic behavior of AMT1;3 spots. Glutamine synthetase (GS) is a key enzyme in ammonium assimilation and recycling in plants. In *Arabidopsis*, *GLN1;2* is one of the genes encoding a GS1 isoform. When *GLN1;2* is knocked out, the internal ammonium level is increased (22). Using SIET and ^{15}N analysis, we confirmed that NH_4^+ uptake in *gln1;2* mutants was indeed lower than those in wild type under N-limiting, N-sufficient, or high external-ammonium treatment, demonstrating that an abnormality of ammonium assimilation can affect the external NH_4^+ uptake (Fig. S10 *C and D*). Furthermore, we analyzed the dynamic behavior of AMT1;3-EGFP spots in the *gln1;2* mutant background using VA-TIRFM. We found that, under N-sufficient conditions, the individual spots amassed into clusters with bigger size and higher fluorescence intensity in the mutant, compared with spots in wild type (*P* < 0.05; Fig. 3 *A and B*). However, there was a significant reduction in the overall fluorescence intensity of the proteins on the plasma membrane (Fig. 3 *F and H*), suggesting the internal ammonium accumulation can promote internalization of AMT1;3-EGFP. When *gln1;2* mutants were treated with high ammonium for 30 min, heavier clustering of the individual spots occurred (Fig. 3 *A and B*) compared with those in wild type, and only 25.1 ± 1.2% of overall fluorescence remained on the plasma membrane (Fig. 3 *G and H*). Western blot analysis further confirmed that, in *gln1;2* mutants, the AMT1;3-EGFP protein underwent some degrees of degradation under high-ammonium stress (Fig. S9). Collectively, our data suggest that the ammonium-dependent regulation of AMT1;3 clustering and internalization provides a fast and efficient way of controlling AMT1;3 activity to avoid cellular ammonium toxicity.

Although the number of transporter molecules in the plasma membrane, which is closely linked to transport capacity, can be regulated by endocytosis and recycling (23), the molecular mechanisms that control the endocytic trafficking of AMTs are not defined. Previous studies indicate that internalization of molecules can occur not only through the classical clathrin-mediated pathway but also through clathrin-independent routes (24). In our study, the internalization time of spots differed significantly, with fast-spot internalization requiring only about 0.66 s, and slow-spot internalization requiring about 6.8 s (Fig. 3I), with a 10-fold increment in protein endocytic rate. This large discrepancy in the time of AMT1;3 internalization suggested that

AMT1;3 internalization may occur through more than one endocytic pathways.

To test this hypothesis, we examined AMT1;3 internalization in the *chc2* mutants, which are defective in bulk endocytosis, as well as in internalization of prominent plasma membrane proteins (25). In *chc2*, we found that the internalization of AMT1;3-EGFP spots in N-sufficient conditions was inhibited and the spots amassed into clusters with larger spot size and higher fluorescence intensity (Fig. 4 *A, I, and J* and Movie S4), compared with that in wild type (*P* < 0.05). Under high-ammonium treatment, the internalization of AMT1;3-EGFP was nearly halted, and the spot size and fluorescence intensity were significantly increased compared with that in wild type (*P* < 0.01; Fig. 4 *B, I, and J*). Western blot analysis confirmed that AMT1;3-EGFP was relatively stable under high ammonium in the *chc2* mutant (Fig. S9). Furthermore, our phenotyping experiment indicated that *chc2* mutant *Arabidopsis* seedlings were more susceptible to ammonium toxicity (Fig. S11 *A and B*). In addition, we found that treatment with tyrphostin (tyr) A23, a specific inhibitor of clathrin-dependent endocytosis (26), can reduce the internalization of AMT1;3 spots and resulted in AMT1;3-EGFP coalescing into larger particles with an increased spot size and fluorescence intensity both under N-sufficient conditions (Fig. 4 *C, I, and J* and Movie S4) and high-ammonium treatment (Fig. 4 *D, I, and J* and Movie S5), similar to the results in the *chc2*
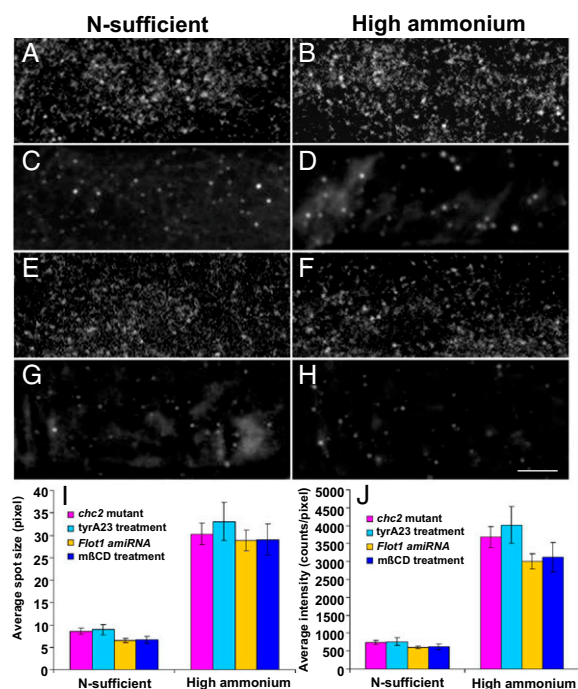

Fig. 4. Inhibition of AMT1;3-EGFP spot dynamics by disrupting endocytic pathways. (*A and B*) Representative VA-TIRFM images of AMT1;3-EGFP spots in the *chc2* mutant background under N-sufficient conditions (*A*) and high-ammonium stress (*B*). (*C and D*) Representative VA-TIRFM images of AMT1;3-EGFP spots in the presence of clathrin inhibitor tyrA23 under N-sufficient conditions (*C*) and high-ammonium stress (*D*). (*E and F*) VA-TIRFM image of AMT1;3-EGFP spots under *Flot1 amiRNA15-5* background under N-sufficient conditions (*E*) and high-ammonium stress (*F*). (*G and H*) VA-TIRFM image of AMT1;3-EGFP spots in the presence of membrane microdomain inhibitor mβCD under N-sufficient conditions (*G*) and high-ammonium stress (*H*). (Scale bars: *A–G*, 1 μm.) (*I and J*) Analysis of the average size (*I*) and fluorescence intensity (*J*) of AMT1;3-EGFP fluorescent spots when endocytosis was disrupted under N-sufficient conditions and high-ammonium supply (*n* = 200). The data were based on analysis of three independent replicates. Values given are means ± SD.
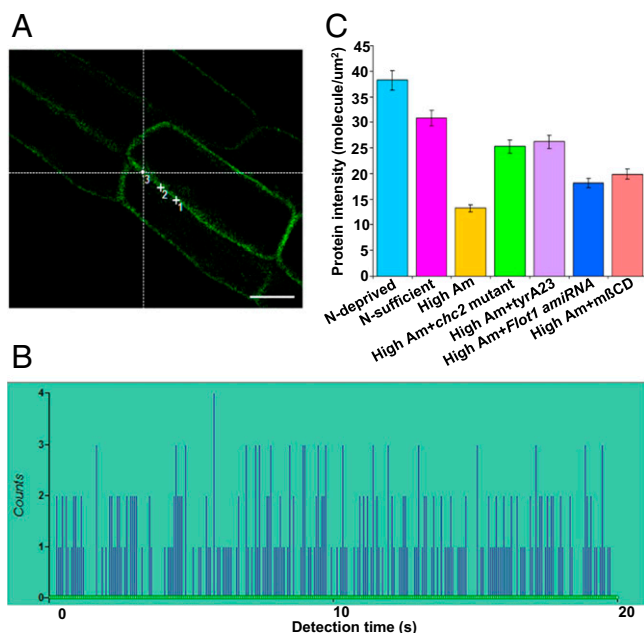
Fig. 5. FCS measurement of AMT1;3-EGFP density in plasma membrane. (*A*) Typical image showing our selection of the FCS measurement region. (Scale bar: 10 μm.) (*B*) Representative graph of fluorescence intensity fluctuation (or counts) of AMT1;3-EGFP during the detection time under N-sufficient conditions. (*C*) Distribution of AMT1;3 transporter density in *Arabidopsis* root cells under different conditions. In N-deprived seedlings, the density of AMT1;3 transporters was about 38 molecules per square micron. Under N-sufficient conditions and high-ammonium stress, the density decreased to about 31 molecules and about 13 molecules per square micron. In the *chc2* mutant background or by tyrA23 treatment under high-ammonium stress, the density increased to about 25 molecules or 26 molecules per square micron. In the *Flot1 amiRNA15-5* line or by mβCD treatment under high-ammonium >stress, the density increased to 18 molecules or 19 molecules per square micron. The data came from three separate replicates. Am, ammonium.

mutant. Indeed, a similar phenomenon was reported previously, showing that PIN protein clustering was linked to reduced dynamics of PIN proteins in the plasma membrane (27). However, the inactive analog of tyrA23, tyrA51 (28), had no effects on the behavior and fluorescence intensity of AMT1;3 (Fig. S12), indicating the effect of tyrA23 is specific. These results suggested that AMT1;3 may internalize through a clathrin-dependent endocytic pathway.

Besides clathrin-dependent endocytosis, clathrin-independent entry pathways have been reported in plant cells, including the membrane microdomain-associated endocytic pathway (29). Previous proteomics studies revealed a tendency of AMT1 transporters to partition in membrane microdomains (30). However, whether they could be internalized through the membrane microdomain-associated endocytic pathway remained to be determined. In the present experiment, we used a *Flot1* (a membrane microdomain marker) *amiRNA15-5* line (31) to analyze whether membrane microdomains were involved in AMT1;3-EGFP internalization. We found that, in the *Flot1 amiRNA15-5* line, the internalization of AMT1;3-EGFP spots was reduced, but the spot size and fluorescence intensity (Fig. 4 *E*, *I*, and *J* and Movie S6) remained almost unchanged under N-sufficient conditions in comparison with that in wild type under N-sufficient conditions (*P* > 0.05). When the seedlings were treated with high ammonium, the spot size and fluorescence intensity (Fig. 4 *F*, *I*, and *J* and Movie S7) were similar to those in wild type under high-ammonium conditions (*P* > 0.05). We then used methyl-β-cyclodextrin (mβCD) to affect membrane

microdomain formation (32). After incubation with 10 mM mβCD, the endocytosis of AMT1;3-EGFP was inhibited, but the spot size and fluorescence intensity remained almost the same as controls under N-sufficient condition (Fig. 4 *G*, *I*, and *J*) and high-ammonium treatment (Fig. 4 *H*, *I*, and *J*). All of these results suggested that the membrane microdomain-associated endocytic pathway may be also involved in AMT1;3 internalization.

To further confirm the role of clathrin or membrane microdomains in regulating AMT1;3 endocytic trafficking, we provide three lines of evidence to demonstrate that clathrin and membrane microdomains contributed differently to the internalization of AMT1;3. First, FCS measurements showed that, when the clathrin-dependent endocytic pathways were disrupted in *chc2* mutants or by tyrA23 treatment, the density of AMT1;3 in the plasma membrane was 92% or 100% higher than with just high-ammonium treatment. However, when the microdomain-associated endocytic pathway was impaired in *Flot1 amiRNA15-5* line or by mβCD treatment, the membrane density of AMT1;3 was only 46% or 50% higher than that in high ammonium without inhibitor (Fig. 5 *A–C*), indicating that impairment of the
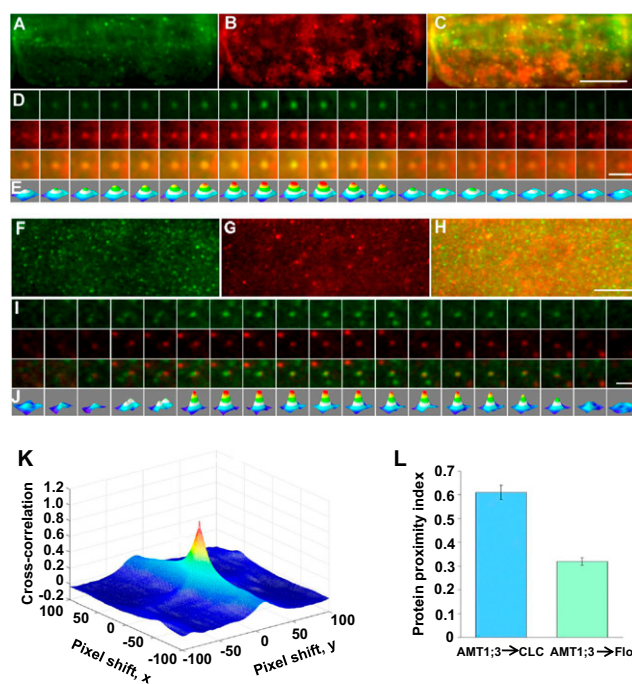

Fig. 6. AMT1;3-EGFP and mCherry-CLC/mCherry-Flot1 spots colocalize at the plasma membrane. (*A* and *B*) Expanding root epidermal cells expressing AMT1;3-EGFP (*A*) and mCherry-CLC (*B*) imaged with VA-TIRFM. (*C*) Merged image of *A* and *B*; the yellow dots represent colocalization, indicating that most of the AMT1;3-EGFP spots colocalize with mCherry-CLC particles. (*D*) An example of real-time dynamic observation of an AMT1;3-EGFP and mCherry-CLC spot. The time series shows AMT1;3-EGFP (*Top*), mCherry-CLC (*Middle*), and a merged image (*Bottom*). (*E*) Three-dimensional luminance plots of the corresponding spots in *D*. (*F* and *G*) Expanding root epidermal cells expressing AMT1;3-EGFP (*F*) and mCherry-Flot1 (*G*) imaged with VA-TIRFM. (*H*) Merged image of *A* and *B*; the yellow dots represent colocalization spots, indicating that only a small fraction of AMT1;3-EGFP spots colocalize with mCherry-Flot1 particles. (*I*) An example of real-time dynamic observation of an AMT1;3-EGFP and mCherry-Flot1 spot. The time series shows AMT1;3-EGFP (*Top*), mCherry-Flot1 (*Middle*), and a merged image (*Bottom*). (*J*) Three-dimensional luminance plots of the corresponding spots in *D*. (*K*) A typical 3D plot of AMT1;3-EGFP and mCherry-CLC cross-correlation vs. pixel shift. (*L*) Mean PPI values showing high (PPI, 0.61 ± 0.03) and low (PPI, 0.32 ± 0.18) colocalization degree of AMT1;3-EGFP and mCherry-CLC/Flot1. Approximately 10–15 cells in at least five different seedlings were measured. (Scale bars: *A–C* and *F–H*, 1 μm; *D* and *I*, 0.25 μm.)

clathrin-dependent endocytic pathway induced heavier accumulation of AMT1;3 at plasma membrane than did impairment of the microdomain-associated endocytic pathway. Second, we examined the colocalization of AMT1;3-EGFP with clathrin or membrane microdomains in plants coexpressing AMT1;3-EGFP/mCherry-CLC (Fig. 6 *A–E*) or AMT1;3-EGFP/mCherry-Flot1 (Fig. 6 *F–J*) based on dual-color fluorescence VA-TIRFM imaging. With the application of a newly developed method (33), we were able to quantify the degrees of colocalization of AMT1;3-GFP/mCherry-CLC and AMT1;3-GFP/mCherry-Flot1. As a result, we found that the protein proximity index (PPI) between AMT1;3 and CLC was 0.61 ± 0.03, but the PPI value between AMT1;3 and Flot1 was significantly lower ($P < 0.01$), at 0.32 ± 0.18 (Fig. 6 *K* and *L*). Similarly, colocalization of endocytic structures between AMT1;3 and CLC/Flot1 in the cytosol was also shown by immunofluorescence (Fig. S13 *A–J*). These results suggest the colocalization of AMT1;3/CLC differed from the colocalization of AMT1;3/Flot1. This conclusion is further supported by the FCCS analysis, which yielded detailed information about the transient and dynamic interaction of AMT1;3 with clathrin or membrane microdomains. We found that the relative cross-correlation amplitude was 0.57 ± 0.03 for AMT1;3-EGFP/mCherry-CLC, but the value was 0.36 ± 0.02 for AMT1;3-EGFP/mCherry-Flot1 (Fig. S14 *A–C*), indicating the interaction between AMT1;3-EGFP and mCherry-CLC was stronger than that between AMT1;3-EGFP and mCherry-Flot1.

Taking these results together, we concluded that the clathrin-dependent endocytic pathway plays a dominant role in AMT1;3 internalization, but the involvement of membrane microdomain-associated endocytic pathway in AMT1;3 endocytosis cannot be excluded.

Materials and Methods

Plant materials, plant culture, drug treatments, image analysis, and FCS and FCCS measurement and analysis are described in *SI Materials and Methods*.

Single-particle fluorescence imaging was performed on an inverted microscope (IX71; Olympus) equipped with a total internal reflective-fluorescence illuminator and a 100× oil-immersion objective (Olympus; NA 1.45) as described (12). The gain of our EM CCD camera was set at 300 throughout all single-particle imaging experiments, and the setting was in the linear dynamic range of the EM CCD camera. Movies of 100–300 frames were captured in a single 200-ms frame.

1. Lanquar V, et al. (2009) Feedback inhibition of ammonium uptake by a phospho-dependent allosteric mechanism in *Arabidopsis*. *Plant Cell* 21(11):3610–3622.
2. Loqué D, et al. (2006) Additive contribution of AMT1;1 and AMT1;3 to high-affinity ammonium uptake across the plasma membrane of nitrogen-deficient *Arabidopsis* roots. *Plant J* 48(4):522–534.
3. Yuan L, et al. (2007) The organization of high-affinity ammonium uptake in *Arabidopsis* roots depends on the spatial arrangement and biochemical properties of AMT1-type transporters. *Plant Cell* 19(8):2636–2652.
4. Gazzarrini S, et al. (1999) Three functional transporters for constitutive, diurnally regulated, and starvation-induced uptake of ammonium into *Arabidopsis* roots. *Plant Cell* 11(5):937–948.
5. Yuan L, Loqué D, Ye F, Frommer WB, von Wirén N (2007) Nitrogen-dependent posttranscriptional regulation of the ammonium transporter AtAMT1;1. *Plant Physiol* 143(2):732–744.
6. Vale RD (2008) Microscopes for fluorimeters: The era of single molecule measurements. *Cell* 135(5):779–785.
7. Zhang W, et al. (2009) Single-molecule imaging reveals transforming growth factor-β–induced type II receptor dimerization. *Proc Natl Acad Sci USA* 106(37):15679–15683.
8. Wan Y, et al. (2011) Variable-angle total internal reflection fluorescence microscopy of intact cells of *Arabidopsis thaliana*. *Plant Methods* 7:27.
9. Miller AE, et al. (2006) Single-molecule dynamics of phytochrome-bound fluorophores probed by fluorescence correlation spectroscopy. *Proc Natl Acad Sci USA* 103(30):11136–11141.
10. Bacia K, Kim SA, Schwille P (2006) Fluorescence cross-correlation spectroscopy in living cells. *Nat Methods* 3(2):83–89.
11. Loqué D, Lalonde S, Looger LL, von Wirén N, Frommer WB (2007) A cytosolic trans-activation domain essential for ammonium uptake. *Nature* 446(7132):195–198.
12. Li X, et al. (2011) Single-molecule analysis of PIP2;1 dynamics and partitioning reveals multiple modes of *Arabidopsis* plasma membrane aquaporin regulation. *Plant Cell* 23(10):3780–3797.
13. Kaiser BN, Rawat SR, Siddiqi MY, Masle J, Glass AD (2002) Functional analysis of an *Arabidopsis* T-DNA "knockout" of the high-affinity NH_4^+ transporter AtAMT1;1. *Plant Physiol* 130(3):1263–1275.
14. Khademi S, et al. (2004) Mechanism of ammonia transport by Amt/MEP/Rh: Structure of AmtB at 1.35 A. *Science* 305(5690):1587–1594.
15. Conroy MJ, et al. (2004) Electron and atomic force microscopy of the trimeric ammonium transporter AmtB. *EMBO Rep* 5(12):1153–1158.
16. Ulbrich MH, Isacoff EY (2007) Subunit counting in membrane-bound proteins. *Nat Methods* 4(4):319–321.
17. Bethani I, Skånland SS, Dikic I, Acker-Palmer A (2010) Spatial organization of trans-membrane receptor signalling. *EMBO J* 29(16):2677–2688.
18. Lenn T, Leake MC, Mullineaux CW (2008) Clustering and dynamics of cytochrome *bd*-I complexes in the *Escherichia coli* plasma membrane *in vivo*. *Mol Microbiol* 70(6):1397–1407.
19. Abrami L, Leppla SH, van der Goot FG (2006) Receptor palmitoylation and ubiquitination regulate anthrax toxin endocytosis. *J Cell Biol* 172(2):309–320.
20. McCann AK, Schwartz KJ, Bangs JD (2008) A determination of the steady state lysosomal pH of bloodstream stage African trypanosomes. *Mol Biochem Parasitol* 159(2):146–149.
21. McLamore ES, et al. (2010) A self-referencing glutamate biosensor for measuring real time neuronal glutamate flux. *J Neurosci Methods* 189(1):14–22.
22. Lothier J, et al. (2011) The cytosolic glutamine synthetase GLN1;2 plays a role in the control of plant growth and ammonium homeostasis in *Arabidopsis* rosettes when nitrate supply is not limiting. *J Exp Bot* 62(4):1375–1390.
23. Pan J, et al. (2009) The E3 ubiquitin ligase SCFTIR1/AFB and membrane sterols play key roles in auxin regulation of endocytosis, recycling, and plasma membrane accumulation of the auxin efflux transporter PIN2 in *Arabidopsis thaliana*. *Plant Cell* 21(2):568–580.
24. Lingwood D, Simons K (2010) Lipid rafts as a membrane-organizing principle. *Science* 327(5961):46–50.
25. Kitakura S, et al. (2011) Clathrin mediates endocytosis and polar distribution of PIN auxin transporters in *Arabidopsis*. *Plant Cell* 23(5):1920–1931.
26. Banbury DN, Oakley JD, Sessions RB, Banting G (2003) Tyrphostin A23 inhibits internalization of the transferrin receptor by perturbing the interaction between tyrosine motifs and the medium chain subunit of the AP-2 adaptor complex. *J Biol Chem* 278(14):12022–12028.
27. Kleine-Vehn J, et al. (2011) Recycling, clustering, and endocytosis jointly maintain PIN auxin carrier polarity at the plasma membrane. *Mol Syst Biol* 7:540–553.
28. Konopka CA, Backues SK, Bednarek SY (2008) Dynamics of *Arabidopsis* dynamin-related protein 1C and a clathrin light chain at the plasma membrane. *Plant Cell* 20(5):1363–1380.
29. Murphy AS, Bandyopadhyay A, Holstein SE, Peer WA (2005) Endocytotic cycling of PM proteins. *Annu Rev Plant Biol* 56:221–251.
30. Morel J, et al. (2006) Proteomics of plant detergent-resistant membranes. *Mol Cell Proteomics* 5(8):1396–1411.
31. Li R, et al. (2012) A membrane microdomain-associated protein, *Arabidopsis* Flot1, is involved in a clathrin-independent endocytic pathway and is required for seedling development. *Plant Cell* 24(5):2105–2122.
32. Yang H, et al. (2013) Sterols and sphingolipids differentially function in trafficking of the *Arabidopsis* ABCB19 auxin transporter. *Plant J* 74(1):37–47.
33. Zinchuk V, Wu Y, Grossenbacher-Zinchuk O, Stefani E (2011) Quantifying spatial correlations of fluorescent markers using enhanced background reduction with protein proximity index and correlation coefficient estimations. *Nat Protoc* 6(10):1554–1567.